Hindawi
Journal of Chemistry
Volume 2021, Article ID 9940577, 11 pages
https://doi.org/10.1155/2021/9940577

Research Article

K_2CO_3-Activated Pomelo Peels as a High-Performance Adsorbent for Removal of Cu(II): Preparation, Characterization, and Adsorption Studies

Zheng Liu and Yuling Wei

School of Environmental Science and Engineering, Xiamen University of Technology, Xiamen, China

Correspondence should be addressed to Zheng Liu; liuzh@xmut.edu.cn

Received 18 March 2021; Accepted 5 June 2021; Published 16 June 2021

Academic Editor: Ibrahim H. Alsohaimi

Activated carbons (ACs) were prepared from pomelo peels by K_2CO_3 activation and used as an adsorbent (PAC) for the removal of Cu(II) from aqueous solutions. BET, SEM, and FT-IR were employed for the characterization of the obtained ACs. The optimum ACs were reported at activation temperature of 850°C, activation time of 60 min, and impregnation ratio of 3, which had a high surface area (1213 m^2/g) and total pore volume (0.57 cm^3/g). The resulting ACs were used for the adsorption of Cu(II) from aqueous solutions in the batch mode and yielded a superior adsorption capacity of 139.08 mg/g. The pH of optimum adsorption was determined as 5. Pseudo first-order model, pseudo second-order model, and intraparticle diffusion model were applied to describe the adsorption processes. The adsorption kinetic data were found to follow the pseudo second-order model. The adsorption isotherms data were analyzed using Langmuir, Freundlich, Temkin, and Dubinin–Radushkevich models. The Langmuir model was found to provide the best fit, and the calculated adsorption capacity was 151.35 mg/g.

1. Introduction

Heavy metal contamination in municipal or industrial wastewater has been a global environmental issue [1]. Most heavy metals (e.g., Cr, Mn, Ni, and Cd) can cause serious damage for ecological systems and public health when their concentrations were in excess [2].

Copper (Cu) is a widely used heavy metal and the main raw material of electroplate, electronics, and cable manufactures [3]. It is an indispensable trace metal for the metabolism and human health in low concentration, but chronic exposure or excessive ingestion may lead to Wilson's disease and damage of digestive system, kidney, or liver [4, 5]. The World Health Organization and European Union propose the maximum level of Cu in drinking water is 2 mg/l [6].

There are various techniques for the treatment of Cu from industrial effluents and wastewaters, such as chemical precipitation [7], flocculation [8], membrane filtration [9, 10], ion exchange [11], electrodialysis [12], and flotation [13]. Among numerous treatment processes, activated carbons (ACs) adsorption is widely used because of its simple design, easy accessibility, and high efficiency [14]. The development of cheaper activated carbon is an important part of promoting its widespread use. Consequently, many recent studies focus on activated carbons produced from alternative low-cost waste biomass, such as hazelnut shell [15], *Ceiba pentandra* [16], bamboo [17], kenaf fiber [18], apricot stone [19], and rice husk [14]. Pomelo (*Citrus maxima*) is a widely cultivated citrus fruit in South China and Southeast Asia. China is a large pomelo producer, and about 1.5–2.5 million tons of pomelo peels are released each year [20]. However, most of pomelo peels are thrown away, giving rise to wasting resources and potential contamination.

Following the "treatment of waste by waste" strategy, this study selected pomelo peels as precursor for preparing ACs (PAC, defined as powdered AC prepared from pomelo peels) with two steps. A nonhazardous chemical (potassium

carbonate, K_2CO_3) was used as an activating reagent. The effects of three activation factors were discussed. The physical and chemical characteristics of the prepared PACs were investigated by BET adsorption, SEM, and FT-IR. Besides, the removal mechanisms of Cu(II) were explored by initial pH effects, adsorption isotherms and kinetic studies.

2. Materials and Methods

2.1. Materials and Regents. Pomelo peels were collected from a local fruit shop. The fresh peels were first dried in the sun naturally, followed by drying at 90°C for 24 h. Then they were smashed to 75–180 μm with a small disintegrator (Yongkang Boou 800Y). All chemicals used were purchased from Sinopharm Group and of analytical grade. Copper sulfate ($Cu_2SO_4{\cdot}5H_2O$) and distilled water were used for preparation of solutions contained Cu(II).

2.2. Preparation of PACs. The preparation processes of PACs were primarily including carbonization and activation [21]. In the carbonization process, the dried meal was put in a tubular stove (Hangzhou Zhuochi SK3-2-10-10) with N_2 flow at 550°C for 2 h. After carbonization, the material was impregnated with K_2CO_3 at different mass ratios (chemical: sample) for 2 h and then the mixture was put in a stove for activation at different activation temperature and different activation time (0.5, 1, 2, and 3 h). After reaction, the ACs (PACs) were repeatedly rinsed with 0.1 M HCl solution and distilled water to neutralize superfluous alkali [22]. Finally, PACs were sieved to 75–180 μm after drying at 90°C for 24 h. PACs obtained under different conditions were denoted as PAC*a*-*b*-*c*, where *a* (°C) was the activation temperature, *b* (*h*) was the activation time, and *c* was the impregnation ratio.

2.3. Characterization of PACs. The textural characterization was manifested by N_2 adsorption-desorption at -196°C using an automated surface area analyzer (TriStar II 3020). The specific surface area was obtained by the BET isotherm equation in the relative pressure of $P/P_0 = 0.995$. The pore size distributions of micropores (<2 nm) were calculated via the density functional theory (DFT) model. The volumes of mesopores and macropores (>2 nm) were calculated via the Barrett–Joyner–Halenda (BJH) method. The characteristics of the micropores were determined from the t-plot method. The SEM micrographs were using a scanning electron microscope (FEI Inspect F50) under high vacuum conditions. The spot size and acceleration voltage were set at 2.5 and 15 kV, respectively. The Fourier transform infrared (FTIR) spectrum of the PACs surface was investigated by Fourier transform infrared spectroscopy (Nicolet 380) in the range of 4000–400 cm^{-1} wavenumbers. FTIR spectra were recorded using KBr pellet technique with 32 scans at a resolution of 4 cm^{-1}.

2.4. Zeta Potential Measurements. The zeta potential of PACs was carried out as follows: 0.1000 g PACs was added to 20 ml of deionized water. Before adding the adsorbent, 0.1 M HCl was used to adjust the pH ranging from 2 to 5. 0.01 M $NaNO_3$ was used to maintain constant ionic strength of solution [23]. Subsequently, the PACs suspension was stirred in a rotary shaker (30°C, 180 r/min) for 24 h and then filtered by 0.45 μm filtering membrane. Finally, the zeta potential of the filtrate was analyzed by a particle size and zeta potential analyzer (Malvern Zetasizer Nano ZS90).

2.5. Adsorption Studies. For the adsorption experiments, the procedures were conducted as follows: 0.0500 g PACs was added to 200 ml of Cu(II) solution. The Cu(II) solution was prepared by adding the corresponding amount of $Cu_2SO_4{\cdot}5H_2O$ to distilled water. The mixed suspension was stirred in a rotary shaker (30°C, 180 r/min) until the adsorption equilibrium was reached. After reaction, the mixed suspension was filtered by 0.45 μm filtering membrane. The concentration of Cu(II) in solution was analyzed by an ICP-OES (PE DV7000). Experiments were carried out in triplicate.

The amount of Cu(II) adsorbed at equilibrium q_e (mg/g) was figured out by

$$q_e = \frac{(C_0 - C_e) \times V}{W}, \quad (1)$$

where C_0 and C_e (mg/l) were the initial concentration and equilibrium concentration of Cu(II), respectively, V (l) was the volume of Cu(II) solution, and W (g) was the mass of PACs.

2.5.1. Effect of the Initial pHs. The effect of pH on the adsorption capacity was investigated by using 0.0500 g of PAC850-1-3 at 30°C. ACs were added to 200 ml of Cu(II) solution (300 mg/l) with the initial pHs of 2, 3, 4, and 5. The pHs of solutions were measured by a desktop acidometer (Sartorius PB-10). The pHs were adjusted by adding of 0.1 M HCl and 0.1 M NaOH solutions to the initial Cu(II) solutions.

2.5.2. Kinetics and Isothermal Studies. Kinetics and isothermal studies were helpful to understand the adsorption mechanisms. Batch experiments of kinetics were carried out at 30°C with 200 ml of Cu(II) solution (100, 200, and 300 mg/l) at pH 5 using 0.0500 g of PAC850-1-3. The sampling and analysis were conducted at specified time intervals. Batch experiments of isotherms were carried out at 30°C with 200 ml of Cu(II) solution (100, 200, 300 400, and 500 mg/l) at pH 5 using 0.0500 g of PAC850-1-3. The sampling and analysis were conducted at equilibrium.

Several common models were used to fit the kinetics data, and isothermal data and average values were adopted in analysis. The equations, linear forms, and plotting methods of these models were listed in Table 1.

In the table, q_e is the amount of adsorbed Cu(II) (mg/g) at equilibrium; q_t is the amount of adsorbed Cu(II) at time t (mg/g); t is the contact time (min); k_1 is the pseudo first-order rate constant (1/min); k_2 is the pseudo second-order rate constant (g/mg·min); k_3 is the intraparticle diffusion

Table 1: Kinetic and isothermal models used in this study.

Kinetics model	Equation	Linear form	Plot
Pseudo first-order model	$dq_t/dt = k_1(q_e - q_t)$	$\ln(q_e - q_t) = \ln q_e - k_1 t$	$\ln(q_e - q_t)$ vs. t
Pseudo second-order model	$dq_t/dt = k_2(q_e - q_t)^2$	$t/q_t = 1/k_2 q_e^2 + 1/qt$	t/q_t vs. t
Intraparticle diffusion model	$q_t = k_3 t^{0.5} + C_i$	$q_t = k_3 t^{0.5} + C_i$	q_t vs. $t^{0.5}$
Isothermal model			
Langmuir model	$q_e = q_m b C_e / 1 + bC_e$	$C_e/q_e = 1/K_L q_m + 1/q_m C_e$	C_e/q_e vs. C_e
Freundlich model	$q_e = k_F C_e^{1/n}$	$\ln q_e = \ln K_F + 1/n \ln C_e$	$\ln q_e$ vs. $\ln C_e$
Temkin model	$q_e = \ln C_e^{A_T} e^{B_T}$	$q_e = B_T + A_T \ln C_e$	q_e vs. $\ln C_e$
Dubinin–adushkevich (D-R) model	$q_e = q_s e^{-\beta\varepsilon^2}$	$\ln q_e = \ln q_s - \beta\varepsilon^2$	$\ln q_e$ vs. ε^2

rate constant (mg/g·min$^{1/2}$); C_i is the intercept of intraparticle diffusion model; b is Langmuir model constant (l/mg); q_m is theoretical maximal sorption value (mg/g); C_e is the equilibrium concentration of Cu(II) (mg/l); K_L is Langmuir coefficient (l/mg); K_F is Freundlich coefficient ((mg/g)×(l/mg)$^{1/n}$); n is adsorption intensity; A_T and B_T are Temkin coefficients; q_s is the adsorption capacities (mol/g); β is the D-R model constant (mol^2/kJ^2); ε is the Polanyi potential, which was obtained by

$$\varepsilon = \mathrm{RT}\ln\left(1 + \frac{1}{C_e}\right). \quad (2)$$

The average relative error (ARE) was used to assess the fitness of kinetic and isotherm models, which was calculated as

$$\mathrm{ARE}(\%) = \frac{1}{n}\sum_{i=1}^{n}\left|\frac{q_{i,cal} - q_{i,\,\mathrm{exp}}}{q_{i,\,\mathrm{exp}}}\right| \times 100, \quad (3)$$

where n is the number of observations in the fit, $q_{i,\,\mathrm{exp}}$ (mg/g) is the observation from experiments, and $q_{i,cal}$ (mg/g) is the estimate from kinetic and isotherm equations.

3. Results and Discussion

3.1. Physicochemical Characteristics of PACs

3.1.1. N_2 Adsorption Isotherms. The adsorption isotherms help to identify the pore structures by adsorbing inert gases. Figure 1 presented the N_2 adsorption-desorption isotherms of PACs prepared under different activation temperatures and impregnation ratios.

According to the isotherm classification proposed by IUPAC, the adsorption isotherms of all samples basically belonged to type I isotherm [24]. When P/P_0 was relatively low (<0.05), the adsorption capacity suddenly increased with the raise of the relative pressure. This phenomenon suggested that there were a huge number of micropores in PACs [25]. In narrow micropores (molecular-sized micropores), enhanced interaction between adsorbent and adsorbate caused micropore filling, which increased the adsorptive capacity at low relative pressures [26].

At higher P/P_0, the isotherms appeared relatively flat, corresponding to monolayer adsorption and micropores with a narrow size range [27, 28]. When the saturation pressure was approached ($P/P_0 > 0.99$), condensation occurred, causing the curve to upwarp. Less obvious hysteresis loops of type H4 were usually found in solids with narrow fissure pores. These loops were not clearly observed in Figure 1, suggesting that PACs also had a few mesopores [14].

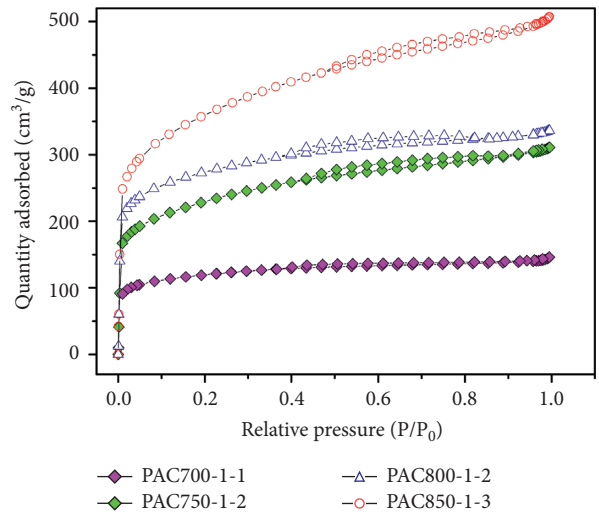

Figure 1: N_2 adsorption-desorption isotherms.

3.1.2. Pore Structure. The adsorption performances of ACs were connected with specific surface areas and pore volumes. Table 2 presented the effect of activation process on specific surface area and pore volume of PACs. Three common operation parameters were discussed, namely, activation temperature, activation time, and impregnation ratio. The specific surface area of pomelo peel was only 2.15 m^2/g. After the physiochemical process, the specific surface areas of PACs were significantly increased, in the range from 771 to 1213 m^2/g.

PAC*a*-1-2s were used to assess the effects of activation temperature (750, 800, 850, and 900°C) on the textural characteristics of PACs. When the temperature was increased from 750 to 850°C, the specific surface areas increased from 771 to 1006 m^2/g. The effects of activation temperature on the micropore volume and total pore volume followed the same trend. Furthermore, when the activation temperature increased from 750 to 850°C, the ratio of the pore volumes (V_{micro}/V_{total}) increased from 48.5% to 72.1%. However, when the activation temperature increased to 900°C, the specific surface area and V_{micro}/V_{total} decreased, which might be because that the consumption of

Table 2: Textural characteristics of PACs.

Material	Surface area	V_{micro}	V_{total}	V_{micro}/V_{total} (%)
Pomelo peel	2.15	—	0.0019	—
PAC750-1-2	771	0.16	0.33	48.5
PAC800-1-2	885	0.25	0.36	69.4
PAC850-1-2	1006	0.31	0.43	72.1
PAC900-1-2	896	0.23	0.37	62.2
PAC850-0.5-2	853	0.25	0.35	71.4
PAC850-1-2	1006	0.31	0.43	72.1
PAC850-2-2	1039	0.32	0.46	69.6
PAC850-3-2	872	0.22	0.36	61.1
PAC850-1-1	819	0.22	0.35	62.9
PAC850-1-2	1006	0.31	0.43	72.1
PAC850-1-3	1213	0.42	0.57	73.7

K_2CO_3 increased and the internal structure of PACs was destroyed by collapsing. These results were inferred that the appropriate temperature was helpful to the generation of new pores. During the formation of holes, the main reactions were as follows [29]:

$$K_2CO_3 + 2C \longrightarrow 2K + 3CO \; K_2CO_3 \longrightarrow K_2O + CO_2 \; K_2O + C \longrightarrow 2K + CO \quad (4)$$

When the activation temperature was over the gasification temperature of potassium (770°C), the gaseous potassium could access the inside of material and consume the carbon atoms on the skeleton, which produced fresh pores.

PAC850-*b*-2s were used to assess the effects of activation time (0.5, 1, 2, and 3 h) on the textural characteristics of PACs. It was obvious the surface areas first rose then declined with increasing activation time. With the increasing activation time, more new holes were constantly generated, resulting in an increasing surface area and pore volume. But with much longer time, excessive burning of pores would occur, and some formed carbon could be enlarged or destroyed, resulting in elimination of surface area and pore volume.

PAC850-1-*c*s were used to assess the effects of impregnation ratio on the textural characteristics of PACs. From Table 2, it could be see that K_2CO_3 was a very efficient activating agent and activated carbons with high porosity were produced through the activation. Table 2 also showed that the impregnation ratio had a great influence on the formation of pores. The surface area of PACs increased from 819 to 1213 m^2/g with increasing the impregnation ratio from 1 to 3. The effects of the impregnation ratio on the micropore volume and total pore volume followed the same trend. It was widely believed that low impregnation ratio caused inadequate contact between activating agent and carbon [30]. Thus, incomplete activation induced limited generation of pores. As the impregnation ratio increased, sufficient contact improved the activation, which was favorable for enlarging pore volume and pore size [31, 32].

3.1.3. Pore Size Distribution. The pore size distribution was an important clue to reveal the adsorption mechanisms of porous materials. Figure 2 illustrated the pore size distributions of PACs. The pores of adsorbing material were usually divided into three categories: micropore (diameter < 2 nm), mesopore (2–50 nm), and macropore (>50 nm) [33]. It could be seen from Figure 2 that all PACs had narrow pore size distributions, including both micropores and mesopores. Most pores of PACs were composed of micropores with sizes ranging from 0.5 to 2.0 nm. All PACs also contained mesopores with narrow range from 2.0 to 8.5 nm. Moreover, Figure 2 presented PACs prepared at different conditions showed discrepant intensity of peaks. Stronger peaks appeared at micropore and mesopore regions of the sample prepared at higher activation temperature and bigger impregnation ratio.

3.1.4. SEM Analysis. The surface morphologies and structural properties of pomelo peel, carbonized pomelo peel, and PAC850-1-3 were investigated via FE-SEM. Figure 3(a) showed the external surface of pomelo peel was dense, neat, and imperforate. After carbonization, the surface was rougher and had some occasional crevices with few bits of pores (Figure 3(b)). This was probably because high temperature pyrolysis caused most organics (organic acid, cellulose, hemicelluloses, lignin, etc.) in pomelo peel to decompose and volatilize, leaving a small number of pores and the cracked surface of carbon.

On the contrary, PAC850-1-3 showed well-formed pores and honeycomb-like structure (Figure 3(c)). This change confirmed the successful preparation of PACs samples with large surface area and high total volume. The pore structures made possible more solutions to access the inside of PACs and were responsible for providing more active sites for adsorbing metal ions.

3.1.5. FTIR Analysis. The FTIR spectrum can provide valuable information about the functional groups on the surface of the material. Figure 4 gave the FTIR spectrum of pomelo peel and PAC850-1-3. It could be seen that PACs presented less and weaker absorption bands than pomelo peel, implying some functional groups presented in the precursor disappeared after physicochemical treatment.

The absorbance peaks of PAC850-1-3 at about 3410 and 2926 cm^{-1} indicated the presence of the stretching vibration of –OH groups (alcohols, phenols, and carboxylic acids) and C–H groups (alkanes), respectively. The peak at 1556 cm^{-1} could be the characteristics of C=O in the quinone structure. The peak of 1042 cm^{-1} suggested the C–O bonds stretching in some oxygen-containing functional groups. The peak of 673 cm^{-1} was ascribed to the out-of-plane bending of the C–H bonds in the arenes [34]. The absorbance peaks at 872 cm^{-1} were ascribed to the out-of-plane deformation of C–H bonds, which indicated that PAC850-1-3 was more inclined to chemisorption process [35].

3.2. Adsorption Studies

3.2.1. Effect of pH. The pH of the solution and the zeta potential of the surface had been identified as the key factors controlling metal ions adsorption because H^+ could compete

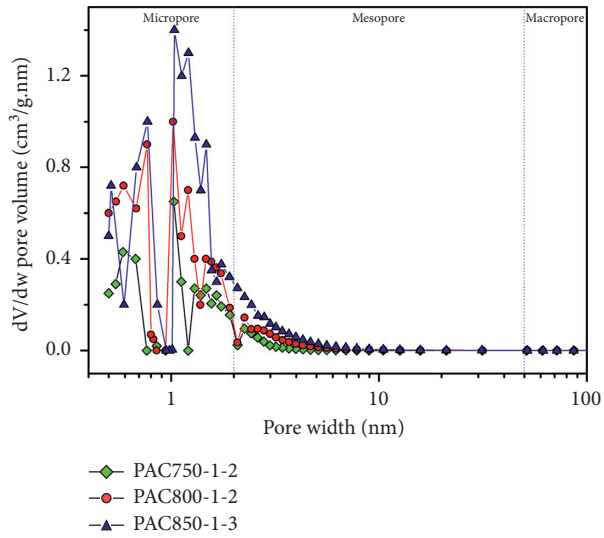

Figure 2: Pore size distribution of PACs.

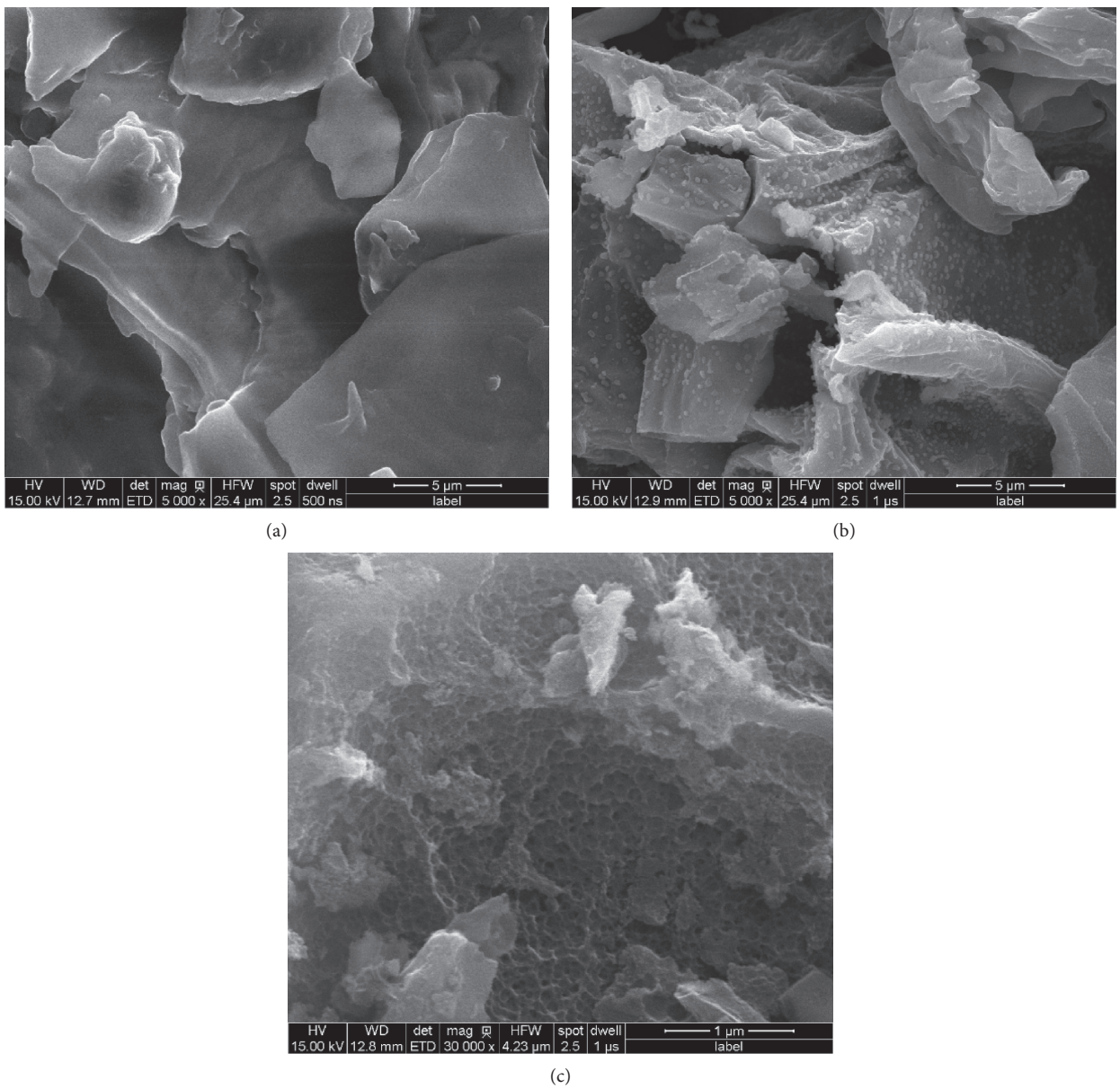

(a) (b)

(c)

Figure 3: SEM of (a) pomelo peel, (b) carbonized pomelo peel, and (c) PAC850-1-3.

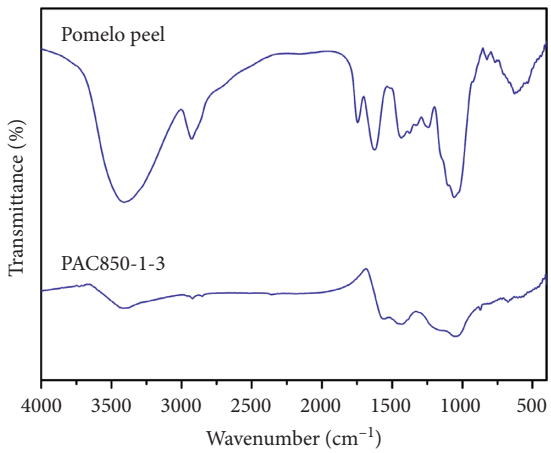

Figure 4: FTIR spectra of pomelo peel and PAC850-1-3.

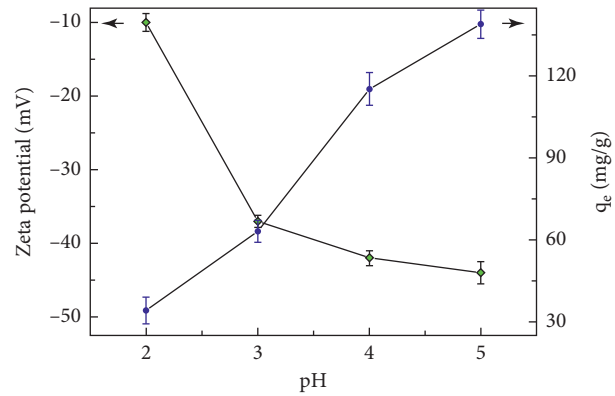

Figure 5: Zeta potential of PAC850-1-3 and the effect of pH on the adsorption capacity of Cu(II) (PACs dose: 0.0500 g; temperature: 30°C; pH: 2, 3, 4, 5; concentration of Cu(II): 100 mg/l). Error bars indicated standard deviation of three replicated experiments.

with metal cations for adsorption sites and the pH of the solution influenced the ionization of functional groups. The zeta potential of PAC850-1-3 and the effect of pH on the adsorption capacity were presented in Figure 5.

As we could see, the zeta potentials of PACs showed negative values in the pH range from 2 to 5. In further evaluation, the zeta potential was roughly −10 mV at pH 2 but fell fast to almost −40 mV at pH 3. As the pH increased from 3 to 5, the zeta potentials slowly descended to the lowest value. Lower zeta potential meant more negatively charged surface, which was in favor of the cations adsorption.

Figure 5 also showed the adsorption capacity of Cu(II) was 34.11 mg/g at pH 2 and then gradually increased to the highest value of 139.08 mg/g at pH 5. Increase in pH beyond 5 could cause precipitation of insoluble metal hydroxides, which would interfere with the adsorption process [36, 37].

When the pH was low, more and faster H^+ could compete with Cu(II) for the adsorption sites in ACs. More H^+ ions made the overall surface charge on PACs become less negative, which impeded the binding of electropositive Cu(II), resulting in lower adsorption. However, with increase in pH, there was a build-up of negatively charged surface, thus making for more Cu(II) removal. The adsorption capacities increased within the pH ranging from 2 to 5, which might be due to partial hydrolyzation of Cu(II). The influence of pH might be attributed to the interactions of Cu(II), $Cu(OH)^+$, and $Cu(OH)_2$ with functional groups at the surface of ACs, which were as follows [38]:

$$\begin{aligned} R-OH_2^+ &\longleftrightarrow R-OH+H^+ \\ R-OH &\longleftrightarrow R-O^- + H^+ \\ R-O^- + Cu^{2+} &\longleftrightarrow R-OCu^+ \\ R-O^- + Cu(OH)^+ &\longleftrightarrow R-OCu(OH) \end{aligned} \quad (5)$$

where R denoted the surface of ACs; $R-O^-$, $R-OH_2^+$, and $R-OH$ denoted different charged hydroxyl functional groups; $R-OCu^+$ and $R-OCu(OH)$ were the formation of the bonding complexes. In addition to the competition between H^+ and Cu(II) at low pH values, fewer deprotonation of functional groups ($R-O^-$, etc.) was adverse to formation of the bonding complexes [39].

Therefore, the best pH for Cu(II) removal was noted to be 5 and all the batch experiments were carried out at this pH.

3.2.2. Adsorption Kinetics. Adsorption kinetics were applied for investigating the efficiency of adsorption at the solid-solution interface. Figure 6 presented that the adsorption of Cu(II) onto PAC850-1-3 demonstrated a rapid velocity at the beginning stage and 50% of the total adsorption occurs within 10 min. This was probably because the adsorption active sites of PACs had not been occupied by Cu(II) at the beginning. Similar result was also reported by Kocabas-Atakli et al. [5]. In that report, the anatase nanoparticles was the adsorbent and the kinetic data of copper also followed the pseudo second-order model. Figure 6 also presented that the adsorbed amount increased with increasing initial concentration of Cu(II). This was probably because higher Cu(II) concentration provided more contact chances between ions and adsorption active sites.

The kinetics data were fitted with three models, which were presented in Figures 7(a)–7(c). Table 3 listed the corresponding kinetics parameters. Clearly, the pseudo second-order model gave higher R^2 and lower ARE, which meant better fit. This indicated that pseudo second-order model was more valid to interpret the adsorption behavior. Similar cases were also reported by other researchers [40, 41]. It could be concluded that chemisorption seemed to be the rate-limiting step which was related to bond forces via electrons sharing or exchange between Cu(II) and PACs.

The intraparticle diffusion model was fitted to understand the diffusion mechanism. As shown in Figure 7(c), all the lines had not passed through the origin, suggesting intraparticle diffusion process was not the rate-limiting step [42]. But intraparticle diffusion played an important part in adsorption process at lower concentration (100 mg/l), for the plots show better linearity. The plots at higher concentration (200 and 300 mg/l) reflected a two-stage process, with initial linear segment followed by plateau (black lines in

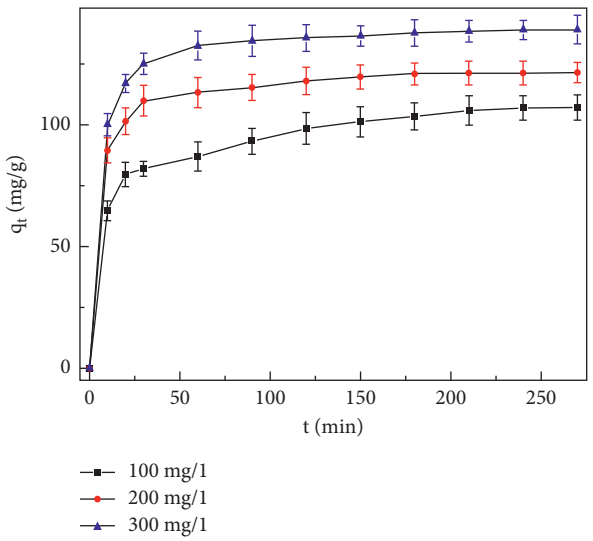

Figure 6: Effects of adsorption time on the adsorption of Cu(II) by PAC850-1-3 (PACs dose: 0.0500 g; temperature: 30°C; pH: 5; volume of of Cu(II) solution: 200 ml; concentration of Cu(II): 100, 200 and 300 mg/l). Error bars indicated standard deviation of three replicated experiments.

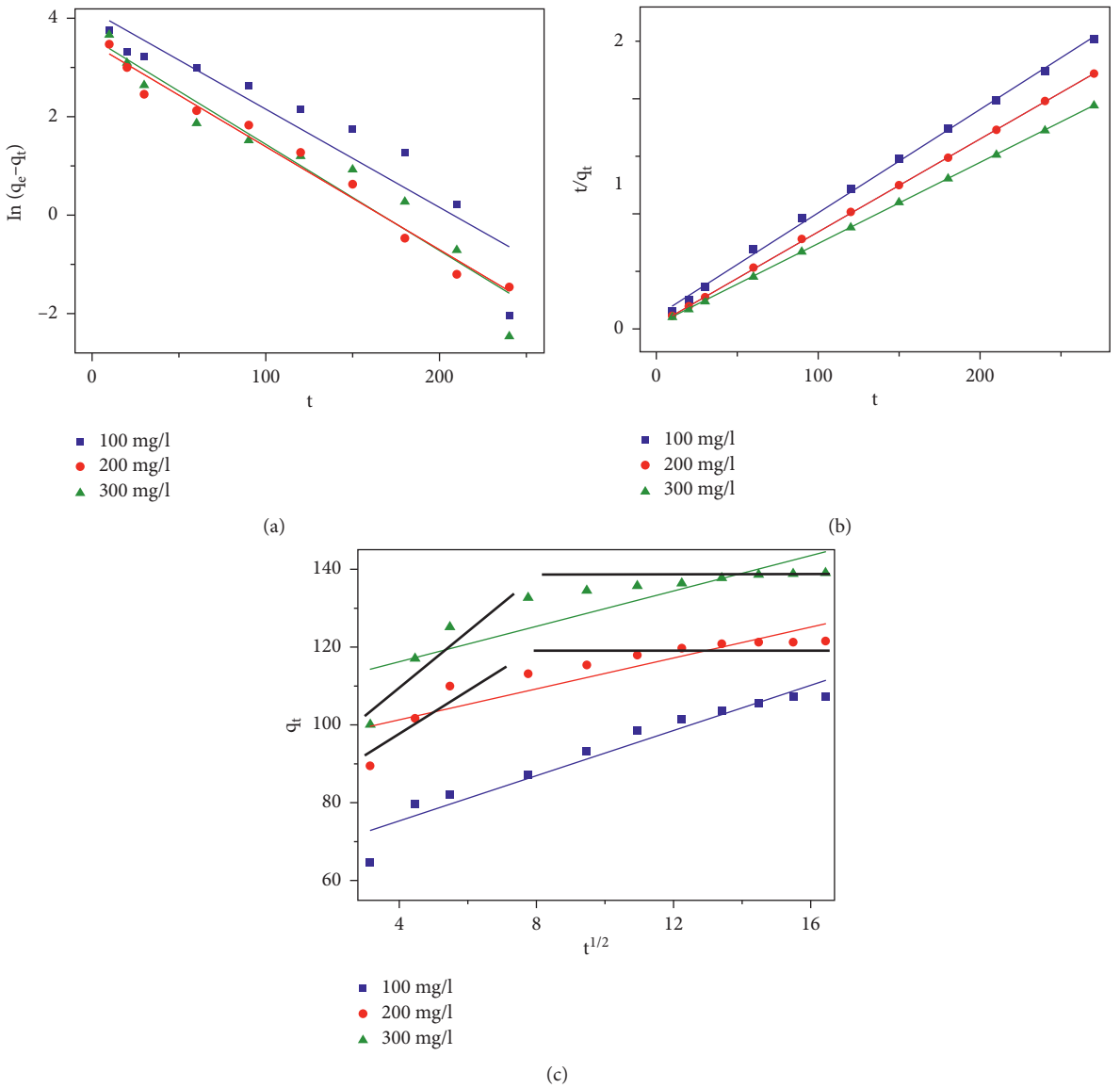

Figure 7: Kinetics of Cu(II) adsorption on PAC850-1-3: (a) pseudo first-order, (b) pseudo second-order, and (c) intraparticle diffusion model (PACs dose: 0.0500 g; temperature: 30°C; pH: 5; volume of of Cu(II) solution: 200 ml; concentration of Cu(II): 100, 200 and 300 mg/l).

Table 3: Parameters of kinetic models for Cu(II) adsorption onto PAC850-1-3.

C_0 (mg/l)				
Pseudo first-order model	$q_{e,cal}$ (mg/g)	k_1 (1/min)	R^2	ARE (%)
100	62.88	0.0199	0.8742	41.3
200	32.63	0.0209	0.9791	73.2
300	36.49	0.0216	0.9369	73.8
Pseudo second-order model				
	$q_{e,cal}$ (mg/g)	k_2 (g/mg·min)	R^2	ARE (%)
100	111.11	0.000749	0.9985	3.7
200	123.46	0.00172	0.9999	1.5
300	140.85	0.00170	1.0000	1.3
Intraparticle diffusion model				
	C (mg/g)	k_3 (mg/g·min$^{1/2}$)	R^2	ARE (%)
100	63.74	2.90	0.9361	4.0
200	93.42	1.98	0.7993	3.6
300	107.12	2.27	0.7389	3.8

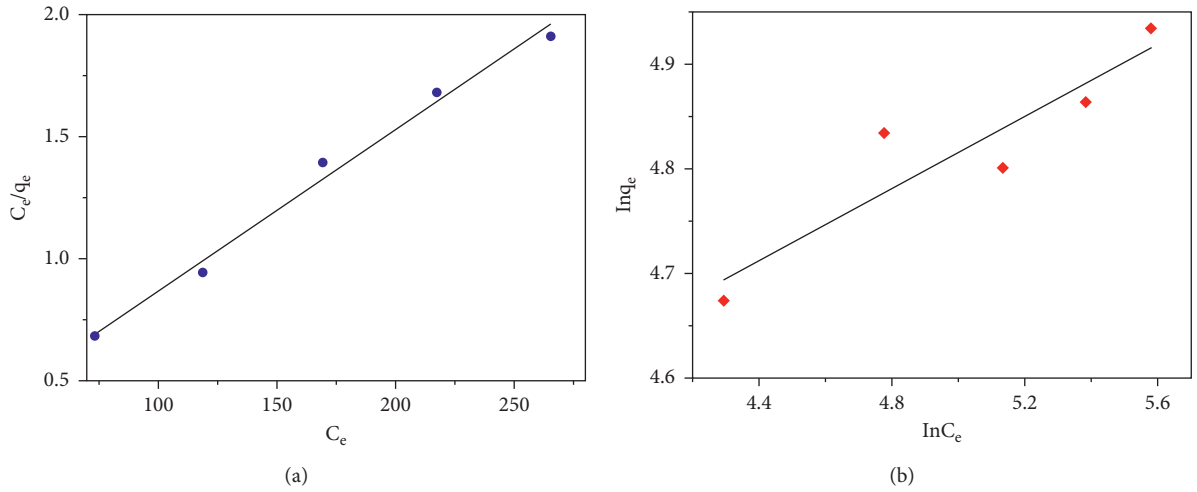

Figure 8: Adsorption isotherms of Cu(II) adsorption on PAC850-1-3: (a) Langmuir and (b) Freundlich (PACs dose: 0.0500 g; temperature: 30°C; pH: 5; volume of of Cu(II) solution: 200 ml; concentration of Cu(II): 100, 200, 300 400 and 500 mg/l).

Figure 7(c)). The initial linear segment implied the exterior surface adsorption, which was a comparatively quick stage. Subsequently, the intraparticle diffusion was quickly arrived and continued to about 70 min. Ultimately, 70 min later the adsorption slowly reached equilibrium. This indicated that the adsorption was a comparatively complicated process. The intercepts of fitted lines of this model gave an understanding of the thickness of boundary layer. The Cu(II) adsorption onto PACs at higher concentration showed greater boundary layer effect.

3.2.3. Adsorption Isotherms. Isothermal adsorption test is a very important way to understand the equilibrium relationship between adsorbate and adsorbent systems at a given temperature. They are also critical for improving the use of adsorbents. Different kinds of adsorption isotherm models have been developed to explicate different isotherm adsorption behavior. In this study, four well-known isothermal adsorption models were served to fit the equilibrium data, namely, Langmuir (Figure 8(a)), Freundlich (Figure 8(b)), Temkin models, and Dubinin–Radushkevich (D-R) model.

The Langmuir model is applied successfully in many monolayer adsorption processes [43, 44]. The Freundlich model is an empirical equation describing multilayer adsorption [45, 46]. The Temkin model also represents multilayer adsorption process considering the thermal effect of adsorption [47]. The D-R model can be used to determine whether the adsorption process was performed physically ($E < 8$ kJ/mol) or chemically ($8 < E < 16$ kJ/mol) [48]. The mean adsorption energy E (kJ/mol) was expressed as

$$E = \frac{1}{\sqrt{-2\beta}}. \quad (6)$$

Table 4 listed the isotherm parameters. The correlation coefficient R^2 was figured out from the corresponding plots in terms of Table 1. Besides, another separation parameter R_L computed from Langmuir isotherm parameters was given as [49]

Table 4: Adsorption isotherm parameters.

Model	Constants			
	q_m	K_L	R^2	ARE (%)
Langmuir	151.35	0.0320	0.990	3.12
	K_F	n	R^2	
Freundlich	52.16	5.804	0.843	3.03
	A_T	B_T	R^2	
Temkin	20.94	19.18	0.840	3.04
	q_s	β	R^2	
D-R	0.00327	$-2.219E-09$	0.845	3.03

Table 5: The comparison of absorption capacity for Cu(II) by PACs and other biomaterials.

Biomaterials	Adsorbent dose, g/ml	pH	q_m, mg/g	Best fit isotherms model	References
Sacha inchi shell	0.1/50	6.00	9.699	Langmuir	[50]
Tomato waste	0.2/50	2–8	22.37	Langmuir	[51]
Beech wood	Unrecorded	4.6–5.0	11–14	Unrecorded	[52]
Lyophilized-bleached almond shell	0.2/50	6	28.7	Langmuir	[53]
Rice straw	0.1/1000	5	29.8	Langmuir	[54]
Lobster shell	0.2/100	2–6	71.4	Langmuir, Freundlich	[55]
Kenaf fiber	0.1/20	5	57.14	Langmuir	[18]
Hazelnut shell	1.0/100	5.0	200	Langmuir, Freundlich	[56]

$$R_L = \frac{1}{1 + C_{0,\max} K_L}, \quad (7)$$

where $C_{0,\max}$ (mg/l) was the highest initial concentration in solution (here $C_{0,\max} = 300$) and K_L (l/mg) had been defined in (2). R_L was an indicator showing the adsorption process was desirable if $0 < R_L < 1$.

Figure 8(a) and Table 4 suggested that Langmuir model fitted better with the isothermal adsorption data ($R^2 = 0.990$ and ARE = 3.12%), when compared to the rest of models. This meant that if a Cu(II) occupied a position, no further adsorption could occur in that site. According to Langmuir model, the maximal monolayer adsorption capacity was calculated to be 151.35 mg/g. It indicated that this adsorbent was a more efficient absorbent than many other biomaterials in Table 5. R_L was calculated to be 0.0943, indicating favorable adsorption of Cu(II). The Freundlich coefficient n also measured the favorability of the adsorption process. In this study, n (5.804) was between 1 and 10, also suggesting favorable adsorption of Cu(II) [16, 57]. Furthermore, D-R model showed that the adsorption of Cu(II) onto PACs was supposed to be a chemisorption process because E had 15.0 kJ/mol, which was in line with the result of kinetics study.

4. Conclusions

Pomelo peel was used to produce activated carbons by K_2CO_3 activation. The removal of Cu(II) by produced ACs was studied in this work. The effects of activation temperature, activation time, and impregnation ratio on the performance of Cu(II) removal were examined. It was observed that there was a large amount of micropores in PACs. The best surface area (1213 m^2/g) and total pore volume (0.57 cm^3/g) were from PAC850-1-3. High temperature was helpful to the generation of more new pores. Appropriate activation time was very important to increase the surface area and pore volume. Higher impregnation ratio was favorable for larger surface area, pore volume, and pore size. Most pores of PACs were composed of micropores with sizes ranging from 0.5 to 2.0 nm. The pH value had a major impact on adsorption capacity and the best pH for adsorption was determined as 5.

Batch adsorption studies showed that the resulting ACs yielded a superior adsorption capacity of 139.08 mg/g. The adsorption process followed the pseudo second-order model at different initial concentrations, suggesting chemisorption seemed to be the rate-limiting step. Langmuir model fitted more closely to the equilibrium data of Cu(II) adsorption, which showed the value of Cu(II) adsorption was 151.35 mg/g. K_2CO_3 was corrosive to equipment, but PACs had a large adsorption capacity and might be considered as a high-performance adsorbent for the removal of Cu(II) from industrial effluents.

Data Availability

The data used to support the findings of this study are available from the corresponding author upon request.

Conflicts of Interest

The authors declare that they have no conflicts of interest.

Acknowledgments

This work was supported by Research Climbing Program of Xiamen University of Technology (XPDKQ19015 and

XPDKT20015) and the Education Department of Fujian Province (JAT200473).

References

[1] M. Hua, S. Zhang, B. Pan, W. Zhang, L. Lv, and Q. Zhang, "Heavy metal removal from water/wastewater by nanosized metal oxides: a review," *Journal of Hazardous Materials*, vol. 211, pp. 317–331, 2012.

[2] N. Dhouibi, H. Binous, H. Dhaouadi, and S. Dridi-Dhaouadi, "Hydrodistillation residues of Centaurea nicaeensis plant for copper and zinc ions removal: novel concept for waste re-use," *Journal of Cleaner Production*, vol. 261, 2020.

[3] M. Mushtaq, H. N. Bhatti, M. Iqbal, and S. Noreen, "Eriobotrya japonica seed biocomposite efficiency for copper adsorption: isotherms, kinetics, thermodynamic and desorption studies," *Journal of Environmental Management*, vol. 176, pp. 21–33, 2016.

[4] A. Arezoo, A. Ahmad, R. Mashallah, and A. Meisam, "Removal of heavy metals from industrial wastewaters: a review," *ChemBioEng Reviews*, vol. 4, no. 1, pp. 1–24, 2017.

[5] Z. O. Kocabas-Atakli and Y. Yurum, "Synthesis and characterization of anatase nanoadsorbent and application in removal of lead, copper and arsenic from water," *Chemical Engineering Journal*, vol. 225, pp. 625–635, 2013.

[6] Lenntech, Drinking Water Tandards, 2020, https://www.lenntech.com/applications/drinking/standards/drinking-water-standards.htm.

[7] X. Zhang, J. Tian, Y. Hu et al., "Selective sulfide precipitation of copper ions from arsenic wastewater using monoclinic pyrrhotite," *Science of the Total Environment*, vol. 705, 2020.

[8] Z. Yang, S. Jia, N. Zhuo, W. Yang, and Y. Wang, "Flocculation of copper(II) and tetracycline from water using a novel pH- and temperature-responsive flocculants," *Chemosphere*, vol. 141, pp. 112–119, 2015.

[9] Y. Bao, X. Yan, W. Du et al., "Application of amine-functionalized MCM-41 modified ultrafiltration membrane to remove chromium (VI) and copper (II)," *Chemical Engineering Journal*, vol. 281, pp. 460–467, 2015.

[10] M. Mohsen-Nia, P. Montazeri, and H. Modarress, "Removal of Cu^{2+} and Ni^{2+} from wastewater with a chelating agent and reverse osmosis processes," *Desalination*, vol. 217, no. 1-3, pp. 276–281, 2007.

[11] S. Edebali and E. Pehlivan, "Evaluation of chelate and cation exchange resins to remove copper ions," *Powder Technology*, vol. 301, pp. 520–525, 2016.

[12] C. Peng, Y. Liu, J. Bi, H. Xu, and A. S. Ahmed, "Recovery of copper and water from copper-electroplating wastewater by the combination process of electrolysis and electrodialysis," *Journal of Hazardous Materials*, vol. 189, no. 3, pp. 814–820, 2011.

[13] H. Polat and D. Erdogan, "Heavy metal removal from waste waters by ion flotation," *Journal of Hazardous Materials*, vol. 148, no. 1-2, pp. 267–273, 2007.

[14] C. Dinh Viet, N.-L. Liu, N. Viet Anh, and C.-H. Hou, "Meso/micropore-controlled hierarchical porous carbon derived from activated biochar as a high-performance adsorbent for copper removal," *Science of the Total Environment*, vol. 692, pp. 844–853, 2019.

[15] E. Demirbas, N. Dizge, M. T. Sulak, and M. Kobya, "Adsorption kinetics and equilibrium of copper from aqueous solutions using hazelnut shell activated carbon," *Chemical Engineering Journal*, vol. 148, no. 2-3, pp. 480–487, 2009.

[16] M. M. Rao, A. Ramesh, G. P. C. Rao, and K. Seshaiah, "Removal of copper and cadmium from the aqueous solutions by activated carbon derived from Ceiba pentandra hulls," *Journal of Hazardous Materials*, vol. 129, no. 1-3, pp. 123–129, 2006.

[17] R. Z. Wang, D. L. Huang, Y. G. Liu et al., "Synergistic removal of copper and tetracycline from aqueous solution by steam-activated bamboo-derived biochar," *Journal of Hazardous Materials*, vol. 384, 2020.

[18] M. R. Razak, N. A. Yusof, A. Z. Aris et al., "Phosphoric acid modified kenaf fiber (K-PA) as green adsorbent for the removal of copper (II) ions towards industrial waste water effluents," *Reactive and Functional Polymers*, vol. 147, Article ID 104466, 2020.

[19] M. Kobya, E. Demirbas, E. Senturk, and M. Ince, "Adsorption of heavy metal ions from aqueous solutions by activated carbon prepared from apricot stone," *Bioresource Technology*, vol. 96, no. 13, pp. 1518–1521, 2005.

[20] L. Xiao, F. Y. Ye, Y. Zhou, and G. H. Zhao, "Utilization of pomelo peels to manufacture value-added products: a review," *Food Chemistry*, vol. 351, Article ID 129247, 2021.

[21] S. W. Choi, J. Tang, V. G. Pol, and K. B. Lee, "Pollen-derived porous carbon by KOH activation: effect of physicochemical structure on CO_2 adsorption," *Journal of CO_2 Utilization*, vol. 29, pp. 146–155, 2019.

[22] A. E. Ogungbenro, D. V. Quang, K. A. Al-Ali, L. F. Vega, and M. R. M. Abu-Zahra, "Synthesis and characterization of activated carbon from biomass date seeds for carbon dioxide adsorption," *Journal of Environmental Chemical Engineering*, vol. 8, Article ID 104257, 2020.

[23] D. Eeshwarasinghe, P. Loganathan, and S. Vigneswaran, "Simultaneous removal of polycyclic aromatic hydrocarbons and heavy metals from water using granular activated carbon," *Chemosphere*, vol. 223, pp. 616–627, 2019.

[24] K. S. W. Sing, "Reporting physisorption data for gas/solid systems with special reference to the determination of surface area and porosity," *Pure and Applied Chemistry*, vol. 54, no. 11, pp. 2201–2218, 1982.

[25] J. Du, L. Liu, L. Zhang, Y. Yu, Y. Zhang, and A. Chen, "Waste chrysanthemum tea derived hierarchically porous carbon for CO_2 capture," *Journal of Renewable And Sustainable Energy*, vol. 9, no. 6, 2017.

[26] R. C. Bansal, M. Goyal, Y. Bao et al., "Application of amine-functionalized MCM-41 modified ultrafiltration membrane to remove chromium (VI) and copper (II)," *Chemical Engineering Journal*, vol. 281, pp. 460–467, 2005.

[27] Z. H. Hu, M. P. Srinivasan, and Y. M. Ni, "Novel activation process for preparing highly microporous and mesoporous activated carbons," *Carbon*, vol. 39, no. 6, pp. 877–886, 2001.

[28] S. Uçar, M. Erdem, T. Tay, and S. Karagöz, "Preparation and characterization of activated carbon produced from pomegranate seeds by $ZnCl_2$ activation," *Applied Surface Science*, vol. 255, no. 21, pp. 8890–8896, 2009.

[29] D. W. McKee, "Mechanisms of the alkali metal catalyzed gasification of carbon," *Fuel*, vol. 62, no. 2, pp. 170–175, 1983.

[30] S. J. Li, K. H. Han, J. X. Li, M. Li, and C. M. Lu, "Preparation and characterization of super activated carbon produced from gulfweed by KOH activation," *Microporous and Mesoporous Materials*, vol. 243, pp. 291–300, 2017.

[31] W. Han, X. Wang, M. Zhu et al., "Melamine modification of spherical activated carbon and its effects on acetylene hydrochlorination," *Journal of Wuhan University of Technology-Materials Science Edition*, vol. 29, pp. 1147–1151, 2014.

[32] J. Li, K. Li, T. Zhang et al., "Development of activated carbon from Windmill palm sheath fiber by KOH activation," *Fibers and Polymers*, vol. 17, pp. 880–887, 2016.

[33] Z. Y. Ryu, J. T. Zheng, M. Z. Wang, and B. J. Zhang, "Characterization of pore size distributions on carbonaceous adsorbents by DFT," *Carbon*, vol. 37, no. 8, pp. 1257–1264, 1999.

[34] S. Mishra, S. S. Yadav, S. Rawat, J. Singh, and J. R. Koduru, "Corn husk derived magnetized activated carbon for the removal of phenol and para-nitrophenol from aqueous solution: interaction mechanism, insights on adsorbent characteristics, and isothermal, kinetic and thermodynamic properties," *Journal of Environmental Management*, vol. 246, pp. 362–373, 2019.

[35] M. I. Sabela, K. Kunene, S. Kanchi et al., "Removal of copper (II) from wastewater using green vegetable waste derived activated carbon: an approach to equilibrium and kinetic study," *Arabian Journal of Chemistry*, vol. 12, no. 8, pp. 4331–4339, 2019.

[36] H. Demiral and C. Güngör, "Adsorption of copper(II) from aqueous solutions on activated carbon prepared from grape bagasse," *Journal of Cleaner Production*, vol. 124, pp. 103–113, 2016.

[37] J. Zhang, H. Fu, X. Lv, J. Tang, and X. Xu, "Removal of Cu(II) fromaqueous solution using the rice husk carbons prepared by the physical activation process," *Biomass and Bioenergy*, vol. 35, no. 1, pp. 464–472, 2011.

[38] X. Wang, X. Liang, Y. Wang et al., "Adsorption of Copper (II) onto activated carbons from sewage sludge by microwave-induced phosphoric acid and zinc chloride activation," *Desalination*, vol. 278, no. 1-3, pp. 231–237, 2011.

[39] F. Bouhamed, Z. Elouear, and J. Bouzid, "Adsorptive removal of copper(II) from aqueous solutions on activated carbon prepared from Tunisian date stones: equilibrium, kinetics and thermodynamics," *Journal of the Taiwan Institute of Chemical Engineers*, vol. 43, no. 5, pp. 741–749, 2012.

[40] D. Kołodyńska, R. Wnętrzak, J. J. Leahy, M. H. B. Hayes, W. Kwapiński, and Z. Hubicki, "Kinetic and adsorptive characterization of biochar in metal ions removal," *Chemical Engineering Journal*, vol. 197, pp. 295–305, 2012.

[41] A. Tomczyk, Z. Sokołowska, and P. Boguta, "Biomass type effect on biochar surface characteristic and adsorption capacity relative to silver and copper," *Fuel*, vol. 278, Article ID 118168, 2020.

[42] H. Demiral and G. Gündüzoğlu, "Removal of nitrate from aqueous solutions by activated carbon prepared from sugar beet bagasse," *Bioresource Technology*, vol. 101, no. 6, pp. 1675–1680, 2010.

[43] P. Y. Ramos, M. T. Munaro, C. C. Triques et al., "Biosorption of binary heavy metal systems: phenomenological mathematical modeling," *Chemical Engineering Journal*, vol. 313, pp. 364–373, 2017.

[44] W. D. M. Souza, W. S. Rodrigues, M. M. S. Lima Filho, J. J. F. Alves, and T. M. B. F. Oliveira, "Heavy metals uptake on Malpighia emarginata DC seed fiber microparticles: physicochemical characterization, modeling and application in landfill leachate," *Waste Management*, vol. 78, pp. 356–365, 2018.

[45] C. Wang, L. Boithias, Z. Ning et al., "Comparison of Langmuir and Freundlich adsorption equations within the SWAT-K model for assessing potassium environmental losses at basin scale," *Agricultural Water Management*, vol. 180, pp. 205–211, 2017.

[46] Z. Zaheer, A. Al-Asfar, and E. S. Aazam, "Adsorption of methyl red on biogenic Ag@Fe nanocomposite adsorbent: isotherms, kinetics and mechanisms," *Journal of Molecular Liquids*, vol. 283, pp. 287–298, 2019.

[47] M. I. Temkin and V. Pyzhev, "Kinetics of ammonia synthesis on promoted iron catalyst," *Acta Physival Chemistry*, vol. 12, pp. 327–356, 1940.

[48] T. E. Köse, H. Demiral, and N. Öztürk, "Adsorption of boron from aqueous solutions using activated carbon prepared from olive bagasse," *Desalination and Water Treatment*, vol. 29, pp. 110–118, 2011.

[49] T. G. Kazi, K. D. Brahman, J. A. Baig, and H. I. Afridi, "A new efficient indigenous material for simultaneous removal of fluoride and inorganic arsenic species from groundwater," *Journal of Hazardous Materials*, vol. 357, pp. 159–167, 2018.

[50] B. Kumar, K. Smita, E. Sánchez, C. Stael, and L. Cumbal, "Andean Sacha inchi (*Plukenetia volubilis L.*) shell biomass as new biosorbents for Pb^{2+} and Cu^{2+} ions," *Ecological Engineering*, vol. 93, pp. 152–158, 2016.

[51] A. . Ş. Yargıç, R. Z. Yarbay Şahin, N. Özbay, and E. Önal, "Assessment of toxic copper(II) biosorption from aqueous solution by chemically-treated tomato waste," *Journal of Cleaner Production*, vol. 88, pp. 152–159, 2015.

[52] S. Vitas, T. Keplinger, N. Reichholf, R. Figi, and E. Cabane, "Functional lignocellulosic material for the remediation of copper(II) ions from water: towards the design of a wood filter," *Journal of Hazardous Materials*, vol. 355, pp. 119–127, 2018.

[53] N. Maaloul, P. Oulego, M. Rendueles, A. Ghorbal, and M. Díaz, "Novel biosorbents from almond shells: characterization and adsorption properties modeling for Cu(II) ions from aqueous solutions," *Journal of Environmental Chemical Engineering*, vol. 5, no. 3, pp. 2944–2954, 2017.

[54] A. K. Sakhiya, I. Aier, S. Pathak et al., "Copper(II) removal from aqua solution using rice straw derived biochar," *Materials Today: Proceedings*, vol. 43, pp. 740–745, 2021.

[55] J. C. Ma, W. Huang, X. S. Zhang, Y. C. Li, and N. Wang, "The utilization of lobster shell to prepare low-cost biochar for high-efficient removal of copper and cadmium from aqueous: sorption properties and mechanisms," *Journal of Environmental Chemical Engineering*, vol. 9, no. 1, Article ID 104703, 2021.

[56] D. D. Milenković, P. V. Dašić, and V. B. Veljković, "Ultrasound-assisted adsorption of copper(II) ions on hazelnut shell activated carbon," *Ultrasonics Sonochemistry*, vol. 16, no. 4, pp. 557–563, 2009.

[57] S. Rangabhashiyam, N. Anu, M. S. Giri Nandagopal, and N. Selvaraju, "Relevance of isotherm models in biosorption of pollutants by agricultural byproducts," *Journal of Environmental Chemical Engineering*, vol. 2, no. 1, pp. 398–414, 2014.